Design and analysis of sub-K continuous heat exchanger for dilution refrigerators

Abhishek Verma[1], Milind Atrey[1] and Dipanshu Bansal[1]

[1] Department of Mechanical Engineering, Indian Institute of Technology Bombay, Mumbai, India

E-mail: abhishekverma284@iitb.ac.in, matrey@iitb.ac.in, dipanshu@iitb.ac.in

Abstract. A continuous tube-in-tube heat exchanger (TTHx) is used to pre-cool the concentrated He-3 stream from 700 to 100 mK (or below) using a dilute stream (6.4% He-3 and 93.6% He-4) in a dilution refrigerator (DR). In commercially available DRs, the inner tube carrying the concentrated stream in TTHx is helically wound (H-TTHx) for compactness and to improve the effectiveness. However, in literature, a helically wound inner tube is rarely modeled owing to modeling complexity, and instead, a linear one-dimensional TTHx (L-TTHx) geometry is used. We present the three-dimensional numerical analysis of a compact footprint (50×50×100 mm^3) L-TTHx and H-TTHx, under the constraint that the outlet temperature of the concentrated stream (T_{co}) remains below 100 mK for varying molar flow rate ($\dot{n}$). We further explicitly determine the contribution of viscous heating, Kapitza resistance, and axial and radial conduction on the temperature profile along L- and H-TTHx and identify their relative contribution. We find that for the same $\dot{n}$ for L- and H-TTHx, the temperature decay of concentrated stream along the length of TTHx differs significantly, leading to different T_{co}. Our study highlights the need to go beyond the standard 1D modeling of H-TTHx used in DR as L-TTHx to accurately model the continuous TTHx and determine its effectiveness.

1. Introduction

Six decades after the first proposal of a dilution refrigerator (DR) working below 1K by London *et al.* [1], DRs are now a workhorse of several research institutes spanning the field of quantum mechanics to astrophysics, among others [2, 3]. The main characteristics of DRs are their capacity to maintain a continuous load of several μW at ~10 mK to a few mW at ~100 mK [4]. The heat exchangers employed between still and mixing chamber are indispensable to DRs, since they allow the concentrated He-3 stream to reach below ~30 mK at the inlet of the mixing chamber, where He-3/He-4 dilution process provides the desired cooling power [1, 5–8]. The realistic prediction of cooling power produced in the mixing chamber depends on its inlet temperature, which in turn necessitates the accurate analysis of heat exchangers, which pre-cool the concentrated He-3 entering the mixing chamber.

A continuous tube-in-tube heat exchanger (TTHx) and a set of two or three discrete silver-sintered heat exchangers are typically used in DRs to pre-cool the concentrated He-3 stream entering the mixing chamber (usually ~10 mK) utilizing the dilute He-3/He-4 solution (6.4% He-

3 and 93.6% He-4) rising under osmotic pressure towards the still (maintained at ~700 mK) [9, 10]. The temperature drop from ~700-100 mK typically occurs in the TTHx [9–11] and hence, the heat transfer mechanism in TTHx is required to be modeled specifically for optimal design. In commercially available DRs, the inner tube carrying the concentrated stream in TTHx is helically wound (H-TTHx) for compactness and enhancing its effectiveness [12, 13]. However, an H-TTHx is seldom modeled as a complete 3-D structure owing to its geometric complexity. Instead, a simplified linear concentric TTHx (L-TTHx) model is analyzed [8, 9, 11, 14, 15], which leads to a variation in the temperature profile along the length of the helix, thus preventing accurate prediction of the outlet temperature of concentrated (T_{co}) and dilute (T_{do}) streams. The differences due to modeling of H-TTHx as L-TTHx further affect its effectiveness with increasing flow rates $\dot{n}$, owing to its dependence on T_{co}. In other words, if T_{co} is fixed (constrained to the required cooling power), the two models provide contrasting estimates of the length of TTHx.
In this study, we present the three-dimensional (3-D) finite element analysis of a compact footprint (50×50×100 mm^3, fixed by the space availability in DR) H-TTHx to overcome the above limitations. We further determine the relative contribution of various heat transfer mechanisms, such as conduction, viscous heating, and Kapitza resistance, to the change in the enthalpy of both streams along the flow. A detailed comparison between H-TTHx and L-TTHx, at different flow rates and length of H-TTHx, emphasizes the differences between the two modeling approaches and hence, the need to go beyond the simplified 1-D analysis.

2. Methodology

2.1 Heat transfer in TTHx

TTHx primarily transfers the heat from the concentrated He-3 to the dilute He-3/He-4 stream through the tube wall (assuming negligible contribution from radiation and convection). In the sub-K temperature regime, the solid-fluid boundaries contribute to a significant thermal load (Kapitza resistance) to the flow [6, 9]. Additionally, geometrical impedance of the fluid channel and viscosity of the fluid lead to heating, thus acting as a loss in this process. Consequently, both the viscous effect and Kapitza resistivity, along with conduction (axial and radial), must be incorporated in an accurate analysis of a TTHx.

Mathematically, the physics of a TTHx can be modelled by the following coupled equations [8, 9, 11] as -

$$s_j \nabla\left(k_j \nabla T_j\right) + \eta_j \left(\dot{n} V_j\right)^2 Z_j - \frac{\sigma_j P_j}{4}\left(T_j^4 - T_w^4\right) = \xi_j \dot{n} C_j \nabla T_j \text{ , and} \quad (1)$$

$$s_w \nabla(k_w \nabla T_w) + \frac{\sigma_d P_d}{4}\left(T_w^4 - T_d^4\right) - \frac{\sigma_c P_c}{4}\left(T_w^4 - T_c^4\right) = 0. \quad (2)$$

'Appendix I' enumerates the variables used in the above equations. The model represented by Equations 1 and 2 emulates the actual heat transfer process across two streams through the boundary, with the former for the heat transfer in the concentrated and diluted streams (index *j* denotes the two streams), and the latter for the wall. The initial three terms of Equation 1 effectively capture the effect of conduction, viscosity, and Kapitza resistivity, respectively. The model assumes that all the heat transferred by the concentrated stream is absorbed by the dilute stream [6].

Although the previous studies and their models also evaluated the above equations, they made varied assumptions to simplify the problem. Two assumptions, apart from neglecting the viscous heating and higher-order T-dependence of different thermo-physical constants [8, 15] are reported in the literature. Firstly, TTHx is considered a linear and coaxial tube in the tube

structure [8, 9, 11, 14, 15] as shown in Case B of Figure 1. Secondly, the heat transfer along the flow direction in both the fluid stream and the tube wall is not considered [9, 14]. These generalized assumptions, while valid for the ideal case of an L-TTHx, are inadequate for H-TTHx [10, 12, 13].

2.2 TTHx model parameters

In contrast to the one-dimensional (1-D) equation solved in the literature (modeling H-TTHx by an LTTHx) [8, 9, 11], we perform a comprehensive 3-D analysis of the H-TTHx based on Equations 1 and 2. Figure 1 shows the geometry of H-TTHx and L-TTHx considered in our analysis. In this study, the dimensions of H-TTHx geometry are kept such that it is constrained to a volume of 50×50×100 mm^3, as required in the case of any practical DRs [12, 16]. In addition to the physical requirement for DRs, the compact H-TTHx shown in Figure 1 also satisfies the technical requirement to pre-cool the concentrated stream from 700 mK to 100 mK (or below) at $\dot{n}$ = 200 μmol/s.

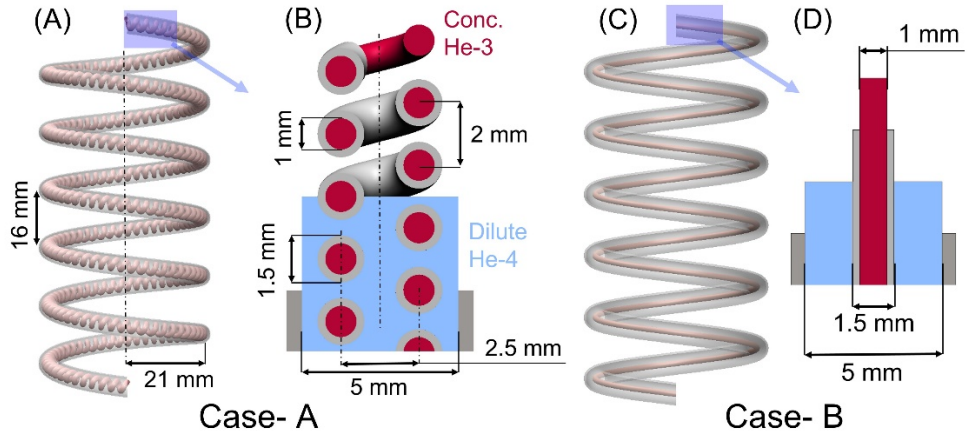

Figure 1. (A) H-TTHx: A representative geometry of double helix heat exchanger - an inner tube is first wrapped into a helix and then inserted into an outer tube. The outer tube, containing a helical inner tube, is again wound into another helix. (B) Exploded view of a section of the H-TTHx showing the helical inner tube inside the outer tube. The choice of the helix parameters is such that a H-TTHx, suitable for pre-cooling concentrated stream from 700 mK to 100 mK (or below) at a flow rate up to 200 µmol/s, is constrained within a volume of 50×50×100 mm^3. (C) L-TTHx: A representative geometry of a concentric tube-in-tube helical heat exchanger- a straight inner tube is inserted into an outer tube. The outer tube, containing a straight inner tube, is then wound into a helix. (D) Exploded view of a section of the L-TTHx showing the straight inner tube inside the outer tube.

For the 3-D analysis, we consider the concentrated fluid to follow the profile of the inner helix. Since heat transfer occurs along the length of the outer helix, the outer helix can be unwrapped without any loss of generality, allowing for the explicit analysis of a straight outer tube containing the helical inner tube. Note that the Reynolds and Dean numbers for concentrated fluid for $\dot{n}$ = 200 μmol/s at the outlet are less than 50 and 30, respectively; hence, the role of helical geometry is to increase compactness and not to induce secondary flows and vortices. For a L-TTHx, the unwrapped outer helix contains a straight concentric inner tube. We exploit the axial symmetry in L-TTHx to further simplify the equations. However, note that the helical geometry of the inner tube in H-TTHx does not permit such symmetry-based simplifications, and we must solve the equation in 3-D. We emphasize that L-TTHx (Case B) does not accurately represent the heat exchange in H-TTHx (Case A) due to a significant difference in the (i) volume of the dilute stream interacting with the concentrated stream (which is ~5.8 times larger in Case B), and (ii) surface

area to volume ratio (which is four times higher for Case A). Nevertheless, the relatively fewer complications associated with symmetry in modelling L-TTHx make it a commonly adopted approach in the literature for analyzing H-TTHx.

Previous studies do not explicitly mention the boundary conditions for TTHx, and instead provide the global boundary conditions at the still and mixing chambers [9, 11, 13]. For this study, we take the temperature at the inlet of the concentrated stream ($T_{\mathrm{c,in}}$) to be the same as the usual still temperature, i.e., 700 mK, while we assume the inlet temperature of the dilute stream ($T_{\mathrm{d,in}}$) to be 30 mK, which is a typical value at the outlet of a set of discrete heat exchangers employed in DRs [9, 11]. We consider that the helical tube is manufactured using cupronickel (Cu-Ni) alloy. We further take T-dependent thermophysical properties, as detailed in Appendix II [8, 9, 11, 17–20]. Using the above-described geometry and material parameters, we implement the equations in the COMSOL Multiphysics [21] finite element solver and compare the temperature profile of the simplified axisymmetric L-THHx model and 3-D H-TTHx model by varying two critical parameters, $\dot{n}$ and the length of H-TTHx ($L_{\mathrm{helix,i/o}}$). We further assess the effectiveness of TTHx and ascertain the relative contribution of each term in Equation 1.

2.3 Model Validation

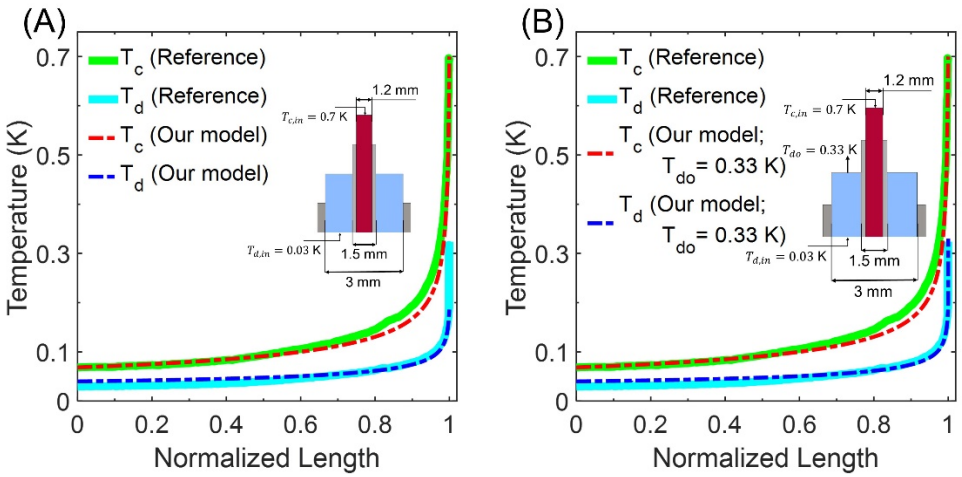

Figure 2. The axisymmetric model is validated against the numerical solution of Equations 1 and 2 specified in Ref. [11]. The thermo-physical properties and dimensions of the geometry are taken from Ref. [11]. (A) The temperature profile, for a flow rate of 60 μmol/s, obtained by our axisymmetric model is compared with data from Figure 6 of Ref. [11]. Since the boundary conditions for L-TTHx are not explicitly mentioned in Ref. [11], a slight deviation occurs in the temperature profile, particularly at the outlet of the dilute fluid. (B) Assuming T_{do} = 0.33 K as a boundary condition, the temperature profile, for both concentrated and dilute streams, obtained from our axisymmetric model closely replicates previous literature [11].

To our knowledge, 3-D models are not available for H-TTHx in the literature for comparison. Therefore, we validate our implementation of the axisymmetric L-TTHx model against the 1-D model of Ref. [11]. The same equations, except for the 3-D geometry, are used for H-TTHx modeling. The dimensions of the inner and outer tubes [11] and boundary conditions are specified in the inset of Figure 2. As we can observe, our results closely replicate the 1-D simulations of Ref. [11] for $\dot{n}$ = 60 μmol/s (see panel A). Since the boundary conditions of Ref. [11] model are not known exactly, we repeat our analysis by changing T_{do} to 0.33 K, which reproduces the temperature profiles near the end points more closely (see panel B); however, small differences still remain due to various unknown geometrical, material, and boundary parameters.

3. Results and Discussions

Here, we present the results of our 3-D HTTx model (Case A) and its simplified L-TTHx model (Case B), shown in Figure 1.

3.1 Temperature profile of the concentrated and dilute stream

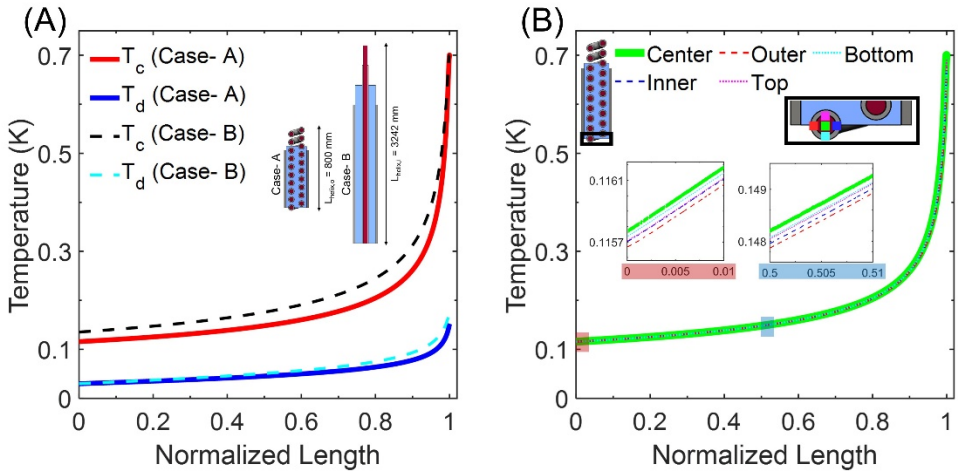

Figure 3. (A) Temperature profile of concentrated and dilute stream at a flow rate of 370 µmol/s along the length for Cases A and B. Note that the temperature profile of the concentrated stream and the dilute stream is normalized along the length of inner tube ($L_{\text{helix,i}}$ = 3242 mm) and the length of outer helix ($L_{\text{helix,o}}$ = 800 mm) respectively. The temperature profile and its decay rate along the length predicted by the L-THHX model deviate from the H-TTHx model and thus predict a larger T_{co}. (B) Temperature profile across the cross-section of the inner helix for Case A (see inset for different radial positions in the cross-section). The variation in a segment of normalized length of 0.01 at two locations (the outlet of the concentrated stream and the middle of the outer helix) shows minimal difference at different radial positions.

Figure 3(A) shows the temperature profiles of the concentrated stream (T_{c}) and dilute stream (T_{d}) for $\dot{n}$ = 370 μmol/s and $L_{\text{helix,i}}$ = 3242 mm, obtained by solving the coupled heat transfer equations for Cases A and B. Evidently, the temperature profile and decay rate obtained from the simplified L-TTHx model deviate significantly. In particular, T_{co} for Case B is ~16.8% larger in comparison to Case A. However, if we compare T_{d}, the difference is negligible since the total temperature rise along the length is relatively small for the dilute fluid due to the large specific heat C_{d} [17]. Figure 3(B) further shows the variation in temperature across the tube's cross-section, which is not accessible in the 1-D modeling. As we can observe, the temperature across the cross-section remains constant. The uniform temperature profile across the cross-section is not as intuitive as it may seem, as Kapitza resistance on the boundary could have led to nonuniform temperature, but the large radial conductivity of the fluid dominates and leads to uniform temperature.

3.2 Factors affecting heat transfer

For the 3-D H-TTHx model (Case A), the contributions of conduction, viscous heating, and Kapitza resistance to the change in enthalpy of the fluid are specified by individual terms in Equation 1, respectively. The contribution of each term is shown in Figure 4. As we can observe that the Kapitza resistance at the boundary of the fluid and solid (wall boundary) predominates over the other contributions from conduction and viscous heating. Hence, the non-significant terms may be omitted in future studies to simplify the problem further. However, these terms would be non-negligible as temperature drops further in the discrete heat exchangers due to a rise in the viscosity.

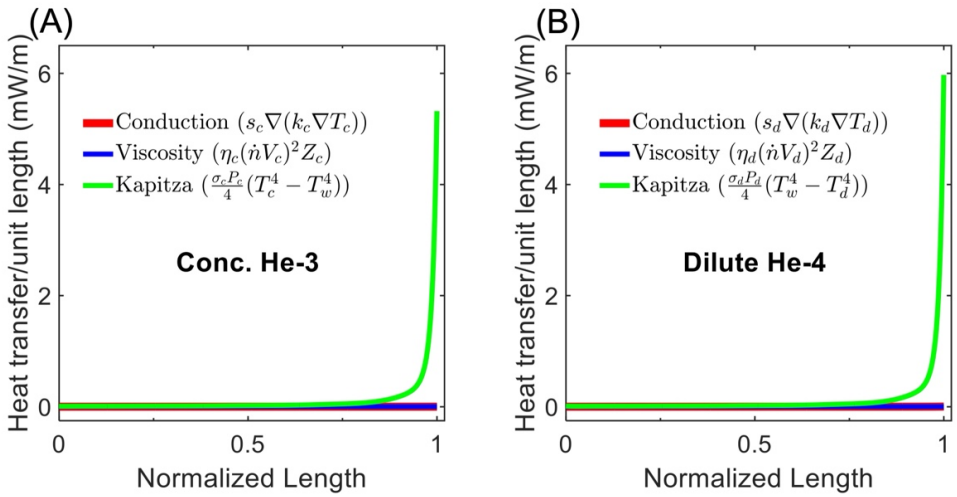

Figure 4. The contribution of each term of Equation 1 in heat transfer from concentrated stream to wall (A) and from wall to dilute fluid (B) for Case A at a flow rate of 370 μmol/s. The enthalpy change of the fluid is primarily driven by heat transfer across the boundary, where heating from Kapitza resistance is largest. Both conduction and viscosity term negligibly affects the heat transfer.

3.3 Effectiveness of TTHx

L-TTHx and H-TTHx must have a sufficiently large contact area to bring T_{co} ≤100 mK. Since T_{co} further depends on $\dot{n}$ (a larger heat ought to be extracted with increasing $\dot{n}$), the required contact area (and consequently length) would be a function of $\dot{n}$ as well. Figure 5(A) compares T_{co} at different $\dot{n}$ for three different lengths of TTHx. For the same $\dot{n}$, the deviation in T_{co} reduces with an increase in the length of the helix, as expected due to increased surface area. Notably, although both models predict nearly equal T_{co} at a small flow rate (~100 μmol/s), the difference increases with an increase in $\dot{n}$ and reaches as high as ~16% above 350 μmol/s for a fixed length of H-TTHx. This can be attributed to the fact that at a lower $\dot{n}$, the available surface area per unit volume is sufficient to exchange heat in L-TTHx. Hence, the improved compactness of H-TTHx in these conditions does not contribute to the performance of the heat exchanger. However, even for lower $\dot{n}$, the compactness of H-TTHx will be preferable to L-TTHx in practical scenarios. We further note that the rate of increase of T_{co} with $\dot{n}$ is higher in Case B. This, as discussed earlier, is due to ~5.8 times larger volume of dilute stream that acts as a sink to absorb comparatively large heat load. Overall, from the results, we can observe that H-TTHx (Case A, $L_{helix,i}$ = 3242 mm) can maintain T_{co} below 100 mK for $\dot{n}$ up to 200 μmol/s, while L-TTHx (Case B, $L_{helix,i}$ = 3242 mm) leads to larger T_{co} values above 150 μmol/s. In other words, modeling of H-TTHx (Case A) as the L-TTHx model (Case B) does not accurately represent its maximum $\dot{n}$ to achieve a given T_{co}.

From the above temperature profiles for different parameters, we further calculate the effectiveness (ϵ) of the heat exchanger using

$$\epsilon = \frac{\dot{n}_c C_c (T_{c,in} - T_{co})}{\dot{n}_J C_{min} (T_{c,in} - T_{d,in})} \quad . \tag{3}$$

Since the heat capacity of the concentrated He-3 is lower than the dilute He-3/He-4 solution, and $\dot{n}$ of both the streams is same, Equation 3 can be simplified as -

$$\epsilon = \frac{T_{c,in} - T_{co}}{T_{c,in} - T_{d,in}} \quad . \tag{4}$$

Figure 5(B) shows that ϵ of H-TTHx is comparable to L-TTHx at smaller $\dot{n}$, but deviates at higher $\dot{n}$, similar to T_{co}. The latter is also evident from Equation 4 as ϵ is directly related to the difference

between $T_{c,in}$ and T_{co}. From the above results, it is evident that at smaller $\dot{n}$ (~100 μmol/s), the modeling of H-TTHx as L-TTHx is sufficient to predict the T_{co} and ϵ, while the differences necessiates the use of 3-D modeling of H-TTHx at higher $\dot{n}$ for accurate predictions.

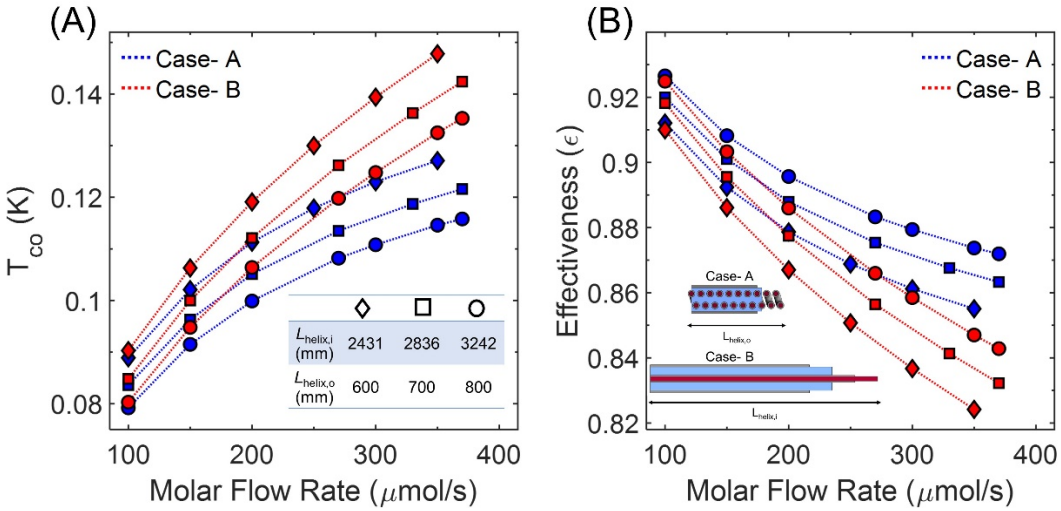

Figure 5. (A) Variation in the outlet temperature of the concentrated stream (T_{co}) at different flow rates and length of helix (L_{helix}) for Cases A and B. T_{co} increases with flow rate at a constant length of inner tube ($L_{helix,i}$) in both cases (shown by dashed line). It is apparent that H-TTHx (Case A, $L_{helix,i}$ = 3242mm) is suitable for a flow rate of 200 μmol/s, while L-TTHx allows only up to 150 μmol/s for T_{co} to remain below 100 mK. (B) Effectiveness of H-TTHx and L-THHx at different flow rates and L_{helix}. As expected from the variation in T_{co} shown in (A), TTHx effectiveness shows a reverse trend. The H-TTHx is more efficient (≥3% compared to Case B) in transferring heat across the fluid domain through the tube boundary at a flow rate above 300 μmol/s.

4. Summary

In summary, we developed a 3-D model of H-TTHx, typically employed in the commercial DRs, to analyze the heat transfer process between the concentrated and dilute streams. We compared our H-TTHx model with the simplified L-TTHx model, commonly studied in the literature, to design and analyze a continuous heat exchanger. The variation in the temperature profile and decay rate along the length of the helix in two different cases (L-TTHx and H-TTHx) confirms that the simplified L-TTHx model falls short in representing the inherent physics of H-TTHx in general and at higher $\dot{n}$ in particular. The deviation in T_{co} and ϵ obtained using the L- and H-TTHx model for different $\dot{n}$ and $L_{helix,i/o}$ substantiates the same. T_{co} and ϵ differ by ~16% and ~3%, respectively for $\dot{n}$ above 300 μmol/s. Furthermore, we explicitly determine the contribution of conduction, viscous heating, and Kapitza resistivity to the rate of enthalpy change. We find that the heating due to Kapitza resistivity is the dominant contribution, consistent with assumptions in the literature. The variation in the result of the two models shown here underscores the necessity to move beyond the L-TTHx model and implement the 3-D HTTx model in future design considerations.

Appendix I

T	Temperature	k	Thermal conductivity [9, 18]

C	Specific heat capacity [17]	σ	Kapitza thermal conductance coefficient [11]
η	Viscosity [8]	$\dot{n}$	Molar flow rate
L	Length of helix	Z	Geometric impedance [8]
V	Molar Volume [19, 20]	s	Cross-section area
P	Perimeter (heat transfer area per unit length)	c	Concentrated stream (99.9% He-3)
d	Dilute stream (6.4% He-3 and 93.6% He-4)	j	Either concentrated or dilute stream
w	Wall	ξ	±1: Either concentrated or dilute stream

Appendix II

$$C_c = \begin{cases} 25.333T - 87.475T^2 + 284.618T^3 - 1097.33T^4 + 1903.57T^5 \ \text{J/mol/K}; & T \le 0.2\ \text{K} \\ -1.2846 + 48.3061T - 228.9698T^2 + 556.0303T^3 & \\ -6666.821T^4 + 315.642T^5\ \text{J/mol/K}; & T \le 0.5\ \text{K} \\ 2.0914 + 3.948T - 4.5068T^2 + 3.37857T^3 - 0.68783T^4\ \text{J/mol/K}; & T \le 1\ \text{K} \end{cases}$$

$$C_d = \begin{cases} 107.16T + 6.1e3T^3 - 3.6e5T^5 - 1.007454e8T^7 & \\ +1.7584e10T^9 - 1.0639e12T^{11} + 2.27312e13T^{13} \ \text{J/mol/K}; & T \le 0.12\ \text{K} \\ -6.2505 + 300.62T - 1.4675e3T^2 + 3.8428e3T^3 & \\ -5.5717e3T^4 + 4.208e3T^5 - 1.28148e3T^6 \ \text{J/mol/K}; & T \le 0.5\ \text{K} \\ 107.16T \ \text{J/mol/K}; & T \le 1\ \text{K} \end{cases}$$

$$k_c = (3.48T^{-1} + 31.4 + 58.1\,T) \times 10^{-4}\ \text{W/m/K}$$

$$k_d = (4.437T^{-0.96} + 4.78e3T^{0.81} - 2.2e2) \times 10^{-4}\ \text{W/m/K}$$

$$k_{wall} = 0.065T^{1.1}\ \text{W/m/K} \qquad \eta_c = (1.81 \times 10^{-7})T^{-2}\ \text{Pa.s} \qquad \eta_d = (5 \times 10^{-8})T^{-2}\ \text{Pa.s}$$

$$\sigma_c = 67\ \text{W/m}^2\text{/K}^4 \qquad \sigma_d = 150\ \text{W/m}^2\text{/K}^4 \qquad Z = \frac{128}{\pi d^4}$$

References

[1] London H, Clarke G and Mendoza E 1962 Physical Review **128** 1992
[2] De Waard A, Bassan M, Benzaim Y, Fafone V, Flokstra J, Frossati G, Gottardi L, Herbschleb C, Karbalai-Sadegh A, Kuit K et al. 2006 Classical and quantum gravity **23** S79
[3] Adams D, Alduino C, Alessandria F, Alfonso K, Andreotti E, Avignone III F, Azzolini O, Balata M, Bandac I, Banks T et al. 2022 Progress in Particle and Nuclear Physics **122** 103902
[4] Zu H, Dai W and De Waele A 2022 Cryogenics **121** 103390
[5] Wheatley J C, Vilches O and Abel W 1968 Physics Physique Fizika **4** 1
[6] Frossati G, Godfrin H, Hebral B, Schumacher G and Thoulouze D 1978 Conventional cycle dilution refrigeration down to 2.0 mK (Physical Society of Japan)
[7] Radebaugh R and Siegwarth J 1971 Cryogenics **11** 368–384
[8] Frossati G 1992 Journal of Low Temperature Physics **87** 595–633
[9] Siegwarth J and Radebaugh R 1971 Review of Scientific Instruments **42** 1111–1119
[10] Uhlig K 1987 Cryogenics **27** 454–457
[11] Shang X S, Miao Z, Cao H q, Wang R, Shao W and Cui Z 2023 International Journal of Refrigeration **146** 381–389
[12] Oda Y, Fujii G, Ono T and Nagano H 1983 Cryogenics **23** 139–147
[13] Uhlig K 2015 Cryogenics **66** 6–12
[14] Siegwarth J and Radebaugh R 1972 Review of Scientific Instruments **43** 197–204
[15] Takano Y 1994 Review of scientific instruments **65** 1667–1674
[16] Ji Z, Fan J, Dong J, Bian Y and Cheng Z G 2022 Chinese Physics B **31** 120703
[17] Radebaugh R 1977 NBS Tech Note, National Bureau of Standards **362** 19
[18] Olson J 1993 Cryogenics **33** 729–731
[19] Kerr E C and Taylor R D 1962 Annals of Physics **20** 450–463
[20] Kerr E C and Taylor R D 1964 Annals of Physics **26** 292–306
[21] COMSOL Multiphysics, v. 5.5. www.comsol.com. COMSOL AB, Stockholm, Sweden